Surface preparations and durability of iron-based shape memory alloy adhesively-bonded joints

Pichler, Niels; Wang, Wandong; Poulis, Johannes A.; Ghafoori, Elyas

DOI
10.1016/j.ijadhadh.2023.103439

Publication date
2023

Document Version
Final published version

Published in
International Journal of Adhesion and Adhesives

Citation (APA)
Pichler, N., Wang, W., Poulis, J. A., & Ghafoori, E. (2023). Surface preparations and durability of iron-based shape memory alloy adhesively-bonded joints. *International Journal of Adhesion and Adhesives*, *125*, Article 103439. https://doi.org/10.1016/j.ijadhadh.2023.103439

International Journal of Adhesion & Adhesives 125 (2023) 103439

Contents lists available at ScienceDirect

International Journal of Adhesion and Adhesives

journal homepage: www.elsevier.com/locate/ijadhadh

Surface preparations and durability of iron-based shape memory alloy adhesively-bonded joints

Niels Pichler [a,b], Wandong Wang [c,a,*], Johannes A. Poulis [d], Elyas Ghafoori [a,e]

[a] Empa, Swiss Federal Laboratories for Materials Science and Technology, Überlandstrasse 129, 8600 Dübendorf, Switzerland
[b] Institute of Structural Engineering, Department of Civil, Environmental and Geomatic Engineering, ETH Zürich, 8093 Zürich, Switzerland
[c] School of Aeronautics, Northwestern Polytechnical University, Xi'an, Shaanxi, PR China
[d] TU Delft – Structural Integrity, Faculty of Aerospace Engineering, Delft University of Technology, Delft 2629HS, The Netherlands
[e] Institute for Steel Construction, Faculty of Civil Engineering and Geodetic Science, Leibniz University Hannover, Hannover 30167, Germany

ARTICLE INFO

Keywords:
Iron-based shape memory alloy
Surface treatment
Durability
Primers and coupling agents

ABSTRACT

Developing a bonded prestressed solution for strengthening structures utilizing an iron-based shape memory alloy (Fe-SMA), is of significant interest. This study is the first systematic investigation of adhesively-bonded Fe-SMA joints to achieve complete cohesive failure, which is an essential prerequisite for bond integrity. The Fe-SMA surface was prepared by combining UV/ozone exposure (UV), sol–gel (SG), and primers (P_C, P_{NC}), and the failure mode of the joint was investigated using the floating-roller peel test. Furthermore, the joint durability was studied through artificial aging using a salt spray cabinet. Cohesive failure was obtained for all investigated adhesives, and the effect of every surface preparation step was described. The application of sol–gel was found to be a crucial step in obtaining complete adhesive failure.

1. Introduction

The use of iron-based shape memory alloys (Fe-SMAs) as civil structural strengthening components has received much attention in recent years [1–4]. These alloys are of particular interest as reinforcement components because of their low cost, good mechanical properties, and unique shape memory effect (SME) feature.

The alloy exhibits the so-called SME thermo-mechanical behavior. This occurs when the alloy changes its crystallographic phase under thermal or mechanical loads. Mechanical loading induces a forward phase transformation and results in permanent deformation, referred to as prestraining. If the prestrained member is subsequently heated and cooled down, the phase transformation is reversed, and the material tends to recover its original size. When the strain recovery is prevented by mechanical constraints, a tensile stress is built up in the alloy. This principle is exploited to induce compressive stresses in the constraining structure, that is, the parent structure to strengthen [2]. A prestrain of 2% was found enough to achieve a maximal recovery stress and representative of the current applications [5]. More details on the recovery stress behavior, transformation stress, and temperatures can be found in [6].

In this regard, the mechanical coupling between the alloy and parent structure is of the highest importance. To date, the load transfer between the prestressed Fe-SMA and its parent structure has been realized using mechanical clamps [2] or nails [3]. These solutions are viable; however, some drawbacks need to be highlighted regarding stress concentration and fatigue life. When Fe-SMA strips are connected to structures using mechanical anchors (e.g., [2,7,8]), the existing stress concentration (as a result of holes) may result in crack initiation in the Fe-SMA or substrate parent structure [1]. An adhesive bond can overcome this issue by providing smoother stress transfer and avoiding stress concentrations owing to holes. It is foreseen that Fe-SMA-bonded solutions would be used more often for prestressed strengthening of structures; therefore, there is a need for studies that fill the knowledge gap on the short-and long-term behavior of Fe-SMA-bonded joints. The adhesive bond could also significantly expand the application field of this alloy, such as in the automotive and aerospace industries.

A first step towards a bonded Fe-SMA joint was undertaken recently [4,9], where lap-shear tests showed promising results, but also raised questions regarding the surface preparation and failure at the adhesive-to-Fe-SMA interface. This interfacial failure mode is known as adhesive failure, in the sense that the adhesion between the adhesive and surface is the limiting factor. This premature failure at the interface should be avoided by carefully preparing the surface to exploit the full strength of the adhesive. Failure should occur inside the bulk adhesive,

* Corresponding author.
E-mail addresses: niels.pichler@empa.ch (N. Pichler), w.wang@nwpu.edu.cn (W. Wang), J.A.Poulis@tudelft.nl (J.A. Poulis), ghafoori@stahl.uni-hannover.de (E. Ghafoori).

https://doi.org/10.1016/j.ijadhadh.2023.103439
Received 17 April 2022; Received in revised form 5 May 2023; Accepted 25 June 2023
Available online 30 June 2023

Nomenclature

A_f	Austenite finish temperature
A_s	Austenite start temperature
G	critical failure energy release rate
M_f	Martensite finish temperature
M_s	Martensite start temperature
P	Load per unit depth
P_C	Primer BR6747-1
P_{NC}	Primer BR6747-1 NCB
ΔA	Crack advance
ΔW_e	Extra elastic energy stored
ΔU_{diss}	Energy dissipated
$\Delta_{machine}$	Crosshead displacement
CFRP	Carbon fiber-reinforced polymer
FTIR	Fourier transform infrared spectroscopy
Fe-SMA	Iron-based shape memory alloy
GB	Grit blasting
SG	Sol-gel AC 103-2
SME	Shape memory effect
UV	UV/ozone exposure

that is, cohesive failure. This is the preferred failure mode in most applications [10–12].

Improving the adhesion and durability of the interfacial adhesive bond is a well-known challenge, and there exists a wide range of methods to improve the adhesion between an adhesive and a metallic substrate [10]. The initial surface texturing is an intuitive method. Grit blasting (GB) [13] can provide good results, but more sophisticated approaches, such as laser gas nitriding [14] have also been studied. The other approach involves the use of chemicals to modify the surface composition prior to bonding. Chemical etching and anodization [15] offer good results; however, these processes involve the use of toxic and environmentally unfriendly agents. Sol–gel technology is an alternative that offers similar performance [16,17], is easier to apply, and more environmentally friendly. In addition, primers have been used as adhesion promoters and corrosion protection products, and have shown promising results for the adhesive bonding of aluminum, titanium, and stainless steel [18]. The AC 130-2 sol–gel (SG) combined with the BR6747-1 chromatic primer (P_C) was found to enhance adhesion and provide a durable bond for austenitic stainless steel [18]. As the Fe-SMA essentially is an austenitic steel (with additional composition elements) [6,19], this surface preparation method is a promising candidate.

It is important to know the specific failure interface when different layers of chemical/polymers are applied to enhance the adhesion in order to pinpoint the weakest part of the joint. The floating-roller peel test [20] (also referred to as the Bell peel test in the literature), takes advantage of the specimen geometry and loads asymmetrically only one side of the joint to reveal the failure interface [21]. This test is a fast and simple method to compare adhesives strength for metal to metal joints. It has also been used with carbon fiber-reinforced polymer (CFRP) to aluminum joints [21], to investigate the effect of aging in CFRP to steel [22] joints, and CFRP to CFRP joints [23].

While the initial bond strength and failure mode are important, their durability is even more crucial. Joints are sometimes exposed to harsh conditions, and their properties must be upheld for long time periods. The most reliable durability test is the full-scale real aging of the joint. Unfortunately, this method is expensive and time consuming. Therefore, accelerated aging processes have been developed to qualitatively assess the corrosion resistance of bonded joints. In this study, a salt spray cabinet was used to expose the joints to a corrosive fog for several weeks based on ASTM B-117 [24].

No study so far has systematically investigated the surface preparation of this novel alloy, and the aim of this study was to investigate the conditions and surface preparations under which adhesively bonded 2% prestrained Fe-SMA joints can be guaranteed to fail cohesively. Cohesive failure is a prerequisite condition for ensuring joint integrity. To this end, multiple surface preparations found to be efficient in the literature were applied to Fe-SMA surfaces, and the joint strength and failing conditions were tested using the floating-roller peel test.

2. Material and methods

The standardized floating-roller peel test was employed (ASTM D-3167 [20]). Its asymmetric specimen design comprises of a thin flexible adherend bonded to a rigid adherend. The test has been shown to primarily load the flexible adherend-adhesive interface [21]. Consequently, Fe-SMA was used as the flexible adherend, while AISI 304 grade steel was used as the rigid adherend. AISI 304 grade steel was selected, as a similar surface preparation was found to provide a durable joint [18]. This ensured that the rigid adherend-adhesive interface would not fail earlier than the Fe-SMA-adhesive interface, which is of interest. Furthermore, the corrosion resistance of AISI 304 grade steel secured the sample integrity during aging process. A variation of surface preparation methods were applied to both adherends prior to bonding. Furthermore, the joints were aged in a salt spray cabinet to assess the durability provided by the surface preparations. This section summarizes the materials used, surface preparation procedures, test method, and data reduction.

2.1. Materials

Fe-SMA (Fe–17Mn–5Si–10Cr–4Ni-1(V, C) %wt.) was provided by Refer AG (Switzerland). The Fe-SMA thickness was 0.5 mm and 50 mm in width. The Fe-SMA was received in hot-rolled state with no heat treatment. A recent study using the same alloy found that the microstructure is fully austenitic [25] and the phase transformation temperatures were reported in [26] to be M_s = -75 ° C, M_f = -90 ° C, A_s = 85 ° C, and A_f = 110 ° C. The AISI 304 grade steel was provided by Salomon's Metalen B.V., as 50 mm wide and 1.5 mm thick plates. This thickness was assumed large enough to provide the necessary stiffness. The adhesives used and their properties are presented in Table 1 and the surface preparation materials in Table 2.

2.2. Test matrix

Ultimately, the investigated surface preparation involves the successive use of two physical processes (grit blasting and UV/ozone exposure (UV)) and the application of two chemical preparations (sol–gel and primer (P_C and P_{NC})). The order of application was GB, UV, SG, and primer. The details of each step are presented in Section 2.3. Different combinations of these processes are used; in this configuration, the effect of each step can be isolated. This results in seven surface preparations in Table 3, where the preparation names indicate each step undertaken, that is, GB+UV+SG+P_{NC} indicates that the plate was grit blasted, exposed to the UV, sol–gel was applied, and the non-chromatic primer was used.

The aging process was only applied to two adhesives, Hysol and Sika, and six of the seven surface preparations, as the amount of Fe-SMA was limited. The final test matrix is presented in Table 3.

2.3. Sample preparation

Fig. 1c shows the subsequent interlayers of the final surface preparation. The floating-roller peel test allows to load primarily this interface and thus identifies the crack location among successive layers.

Table 1
Adhesives selected and curing details according to the manufacturer's datasheets.

Adhesive	Hysol EA 9394	SikaPower 1277	FM 300–2	Araldite 2015
	[27]	[28]	[29]	[30]
Short name	Hysol	Sika	FM 300–2	Araldite
Application	Aerospace	Civil engineering	Aerospace	Civil engineering
Behavior	Brittle	Ductile	Brittle	Ductile
Tensile strength [MPa]	46	30	6.15*	30
Elongation at break [%]	1.66	4	–	4.4
Target thickness [mm]	0.2	0.3	0.6	0.1
Curing temperature [° C]	20	20	121	20
Curing time	3–5 days	24 h	90 min	7 days
Curing pressure	–	–	2.8 bar	–

*Flatwise tensile [29].

Table 2
Surface preparation materials. P_C and P_{NC}, are two versions of the same material, P_{NC} being the non-chromatic version of P_C.

Name	Sol–gel AC 130-2[a] [31]	BR6747-1[b] [32]	BR6747-1 NCB[a] [33]
Short name	SG	P_C	P_{NC}
Purpose	adhesion enhancement	corrosion protection	corrosion protection
Curing temperature [° C]	–	121	121
Curing/drying time	60 min	90 min	90 min

[a]Supplied by Secoa B.V. in The Netherlands.
[b]Supplied by Aerospheres (UK) Ltd.

Table 3
Test matrix. Each combination of surface preparation, adhesive tested, and aging time is represented by a ✓, untested conditions are marked with X. The surface preparation name indicates each step applied to the surfaces, and four samples were tested in each configuration.

Adhesive	Hysol			Sika			FM 300–2	Araldite
Surface preparation \ Weeks aged	0	6	12	0	6	12	0	0
GB*	✓	✓	✓	✓	✓	✓	✓	✓
GB+P_{NC}†	✓	✓	✓	✓	✓	✓	✓	✓
GB+SG‡+P_{NC}	✓	✓	✓	✓	✓	✓	✓	✓
GB+SG+P_C§	✓	✓	✓	✓	✓	✓	✓	✓
GB+UV⋄	✓	✓	✓	✓	✓	✓	✓	✓
GB+UV+SG+P_{NC}	✓	✓	✓	✓	✓	✓	✓	✓
GB+UV+SG+P_C	✓	X	X	✓	X	X	✓	✓

* Grit blasting, † non-chromatic primer, ‡ sol–gel, § chromatic primer, ⋄ UV/ozone exposure

The specimens were manufactured according to the ASTM standard D-3167 [20]. The surfaces were prepared on 50 mm wide plates as shown in Fig. 1a, bonded, and finally cut into four specimens (two in the width, two in the length as the configuration in Fig. 1a), 15 mm in width, by waterjet cutting. All the surface preparations detailed in the following subsections were applied to the plates.

2.3.1. Grit blasting

Both plates were first thoroughly pre-cleaned with acetone cotton wipes to remove as much contaminants as possible. The surfaces were grit blasted in a Pulsar 3 Clemco blasting cabinet. The grit blasting pressure was 6 bar, and the nozzle was kept at 10 ± 0.5 cm in a 45 ° angle to the surface of the plates. The grit blast material was 40 grit glass beads, filtered before being recirculated. The Corublast super glass beads were provided by Leering Hengelo B.V. The AISI 304 grade steel was only grit blasted on one side, both sides of the Fe-SMA plate were grit blasted to equalize the surface warping. After grit blasting, the dust was removed using pressured air and the plates subsequently cleaned with acetone cotton wipes.

In this step, the mechanical treatment of the surface may induce stresses greater than the yield strength. This implies that stress-induced phase transformation of austenite to martensite occurs at the surface, which may alter the surface roughness [34]. It is, however, assumed that the effect on the global surface roughness is negligible compared to the mechanical roughening.

2.3.2. UV/ozone exposure

Some plates were placed in a closed container and exposed to a UV light source of 185 nm and 254 nm, generating ozone and highly active oxygen radicals. The UV light tubes were supplied by UV Technik in Germany and mounted inside a wooden box. This exposure had two purposes: first, to remove any organic compound remaining at the surface [35] and second, to increase the surface free energy due to oxidation [36], resulting in improved surface wetting (see Fig. 2).

To define the optimal exposure time to the UV source, similar to [36], the wetting properties of Fe-SMA surfaces exposed for 0, 3, 5, 10, 15, and 30 min were measured by contact angle measurements on a Technex Cam200/Attension (CAM), as shown in Fig. 2(a). A 5 μ l distilled water droplet was placed on the surface, and the wetting angle was recorded by curve fitting the droplet contour, as shown in Fig. 2(b). Each measurement was repeated five times. The static apparent wetting angles for prestrained and non-prestrained Fe-SMA before and after grit blasting were measured. Based on these results (Fig. 2(a)), the optimal exposure time to the UV source was chosen to be 15 min.

2.3.3. Sol–gel

The sol–gel AC 130-2 coating was applied by brushing, within one hour after either the grit blasting or the UV/ozone exposure according to the manufacturer's technical datasheet [31].

2.3.4. Primers

Both primers were applied according to the same procedure described in the product's technical datasheets [32,33]. This process includes curing at 121 ° C (see Table 2). The primers were applied directly after the sol–gel finished drying, 1 h at room temperature, 20 ° C.

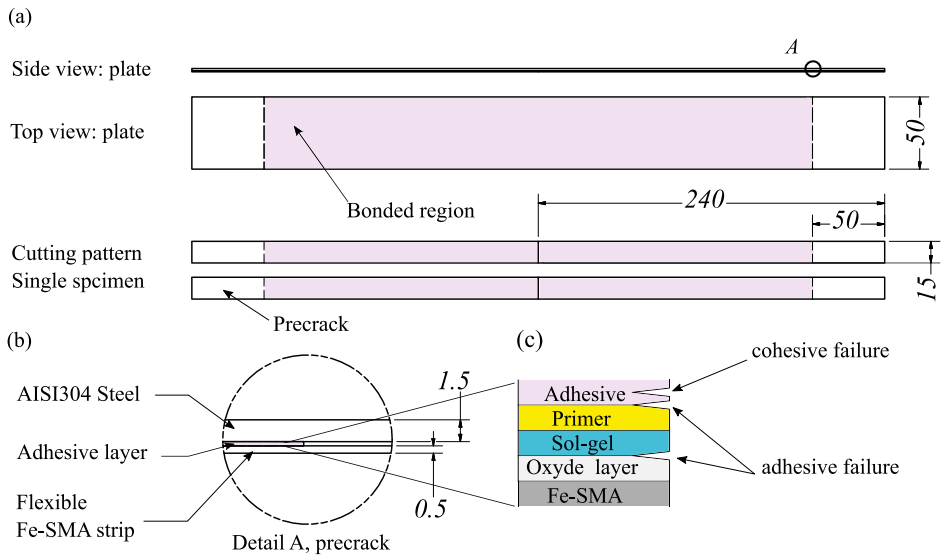

Fig. 1. Plate and specimen dimension and configuration. (a) Prepared plate and configuration of specimens cut into the plate. (b) Details of precrack and bonded plates. (c) The detailed interface between the Fe-SMA and the adhesive is the result of the surface preparation investigated. Failure location indicates the failure mode, adhesive, or cohesive.

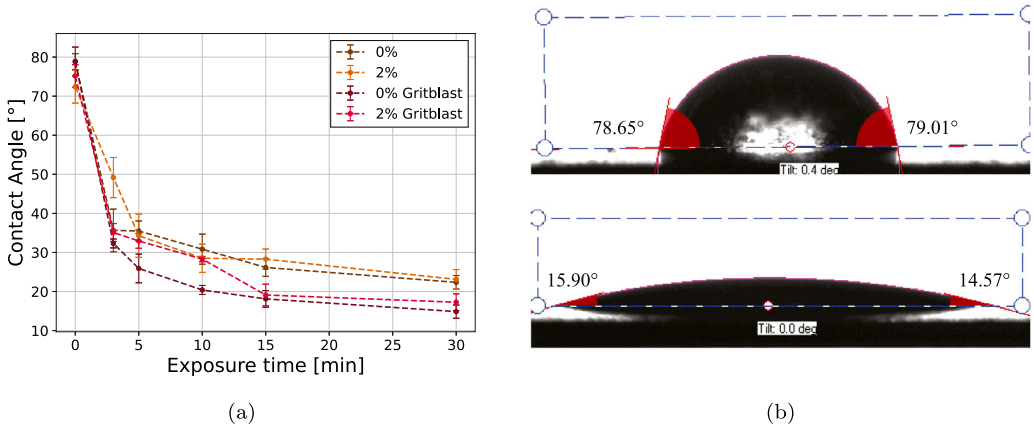

Fig. 2. Contact angle measurement analysis. (a) Contact angle of distilled water as a function of the exposure time to UV/ozone for prestrained and non-prestrained Fe-SMA, and grit-blasted and non-grit-blasted Fe-SMA. (b) Wetting of a distilled water droplet before (top) and after (bottom) 30 min of UV/ozone exposure on non-prestrained grit-blasted Fe-SMA surfaces.

If the primer layer is too thick, the primer's mechanical properties can influence the joint and lead to premature failure [10,37]; therefore, it is critical to control its thickness. However, because of the surface roughness, even before grit blasting, it was not possible to measure the primer thickness. An Extech CG304 Coating Thickness Tester in Eddy-current working principle was used, but no reliable thickness value could be recorded. A Keyence VK-X1000 confocal microscope revealed that the rolling striae amplitude of the Fe-SMA was greater than 20 μ m. Therefore, it was not possible to define a reference point for measuring the thickness. Furthermore, it was observed that the primer formed a multitude of droplets, giving little meaning to the definition of the coating thickness. Through confocal microscopy (see Section 2.5.2), the amplitude range measured with (or without) primer remained unchanged, leading to the conclusion that the droplet thickness was well below 20 μ m.

2.3.5. Prestraining

To develop a prestress, the Fe-SMA needs to be prestrained, bonded, heated to the reverse transformation temperature (A_s), and cooled down. A prestrain of 2 % was found to be enough to achieve a maximal recovery stress and representative of applications of Fe-SMA [5]. Because the primer curing temperature (121 ° C) was higher than A_s, prestraining could only be applied after primer curing.

The 480 mm strips (Fig. 1) were prestrained to 2 % using a Zwick-Roell testing machine with a 250 kN load cell in a displacement-controlled condition with a loading speed of 1 mm/min. A Zwick-Roell BTC-EXMACRO.002 extensometer with ±0.15% uncertainty on the measured length was used to record a nominal strain of 2 %. The initial extensometer arm opening was 180 mm.

2.3.6. Adhesive bonding

The final step of the specimen manufacturing process was adhesive bonding. A 50 mm precrack was created by taping both ends of the Fe-SMA plate with Airtech flashbreaker 1 tape (Fig. 1). Glass beads were added to the adhesive to control the layer thickness, 4% by weight, with a diameter of 90–150 μ m for Araldite, 200–300 μ m for Hysol. In the case of Sika, where glass beads are already included in the product [28]. The adhesives were manually smeared on both substrate surfaces. The adherends were bonded and placed in a mold to control alignment. Finally, a weight of approximately 15 kg was placed at the top. The room temperature was approximately 20 ° C with 70 % relative humidity (RH). The details of the target thickness and curing conditions can be found in Table 1.

For the FM 300-2, a 0.6 mm thick film was applied only to the Fe-SMA surface, and the Fe-SMA was placed onto the AISI 304 grade steel

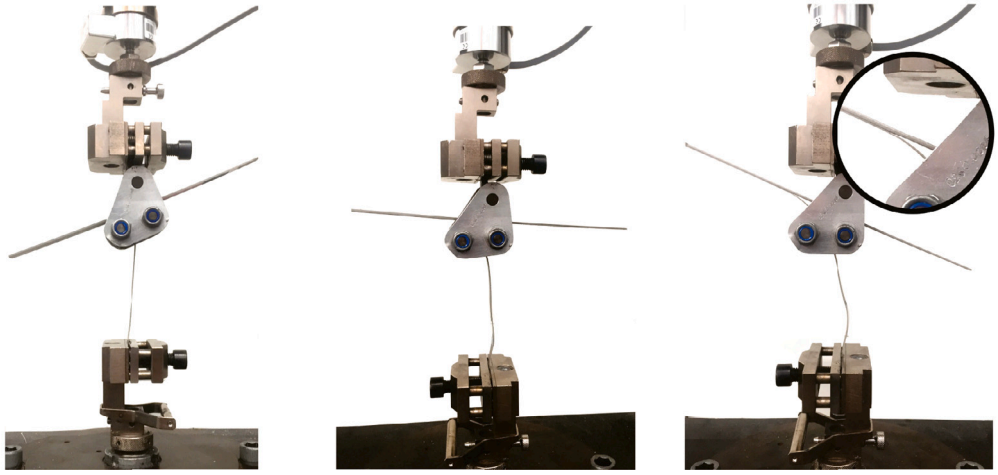

(a) Peel test unfolding correctly, Scenario A.

(b) Peel test unfolding in the limit case, Scenario B.

(c) Peel test unfolding incorrectly, the closeup shows the important noncompliance with the roller, Scenario C.

Fig. 3. Floating-roller peel test scenarios.

plate. The plates were cured in an autoclave at 121 ° C and 2.8 bar for 120 min (30 min ramp and 90 min hold), as specified in the product's technical datasheet [29].

2.4. Test method

2.4.1. Floating-roller peel test

To determine the failure type, the joints were tested using the floating-roller peel test, ASTM D3167 standard [20]. The test measures the load necessary to peel off an adhesively-bonded strip from its adherend. The flexible adherend is peeled through a fixture away from the rigid adherend, as in Fig. 3(a). The test was carried out in a uniaxial Zwick-Roell testing machine with a ±0.2% accuracy, 1 kN load cell, a loading speed of 152 mm/min, and a sampling rate of 10 Hz.

The test can unfold according to three different scenarios depending on the interfacial strength and adherend stiffness. First, the test behaves as expected, as in Fig. 3(a), the flexible adherend complies with the roller radius, and the peel angle is predetermined, hereafter referred to as Scenario A.

Second, the flexible adherend was slightly stiff for the test and interface strength. The rigid adherend rises to a horizontal but stable position, referred to as Scenario B (Fig. 3(b)) [38]. In this case, the flexible adherend still undergoes significant deformation, and the test is regarded as valid.

In Scenario C, the interface strength is too low, the decohesion propagates backward, and the load is transmitted to the crack tip through the elastic bending of the flexible adherend (Fig. 3(c)). This loading was considered to be invalid. However, the determination of the failure type remains valid. This scenario occurs when the interface adhesion is very low, leading to a 100 % adhesive failure.

2.4.2. Aging, salt spray exposure

To assess the joint's durability, Sika and Hysol adhesive joints were subjected to accelerated aging [18,36,39]. The joints were placed in a salt spray cabinet (Liebisch Constamatic Salt Spray chamber) according to the standard ASTM B117-19 [24], at 35 ° C for a duration of 6 and 12 weeks. The NaCl concentration in the water was 5 % by weight.

To prevent the adherends from getting corroded in the chamber and examine only the effect on the interface, the top and bottom face of the samples were coated with a metal paint (Hammerite Metaallak, Akzo Nobel Paints Belgium NV/SA). Only the edges of the joints were exposed to the harsh environment.

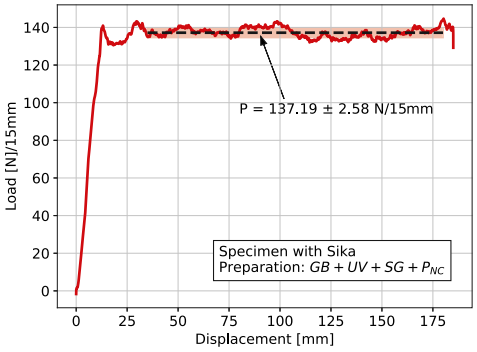

Fig. 4. Example of a typical load displacement curve.

For practical reasons, the specimens had to be placed in a horizontal position. This caused water to flow from the specimen top surface to the bottom of the cabinet through the same path on the specimen edge. It lead to a locally more aggressive corrosion process as water was actively flowing in this location. The effect on the load–displacement curve were limited as the effect were very local and therefore ignored in the results analysis.

2.5. Analysis tools

The different analysis tools and data reduction used to generate the final results are summarized. The load–displacement curve was used to extract the average peel load. Visual assessment, microscopy, and Fourier transform infrared spectroscopy (FTIR) were used to determine the failure mode [40].

2.5.1. Load displacement curve analysis

A typical load displacement curve is presented in Fig. 4. The load is corrected to correspond to a 15 mm width as the machining gave rise

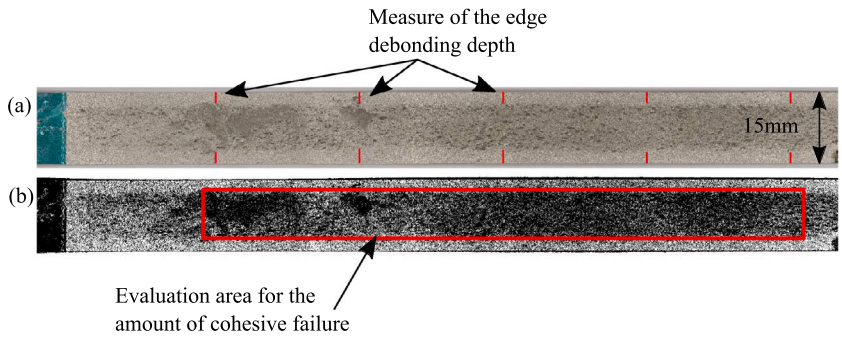

Fig. 5. (a) Fe-SMA fracture surface bonded with Hysol with GB+SG+P_{NC} surface preparation after six weeks aging. (b) Color threshold, cohesive failure in black, and adhesive failure in white.

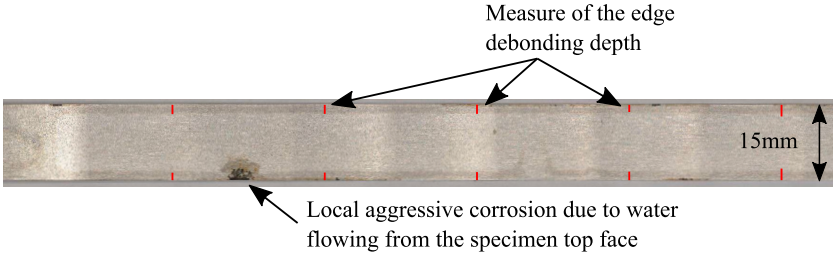

Fig. 6. Fe-SMA fracture surface bonded with Sika and GB+P_{NC} after six weeks aging. The depth debonded by water diffusion is characterized by the darker color of the Fe-SMA.

to slight variations in specimen width. The average load in the region of interest (red box Fig. 4), and the standard deviation were measured for each specimen. Each test was repeated at least four times. Only the mean of the average peel loads and a pooled standard deviation are reported.

2.5.2. Fractography

To determine the failure mode, the fracture surfaces of the Fe-SMA were inspected. Visual inspection was sufficient to detect cases of complete adhesive failure. In such cases, the Fe-SMA surface was entirely stripped of any adhesive, and only the bare metal was visible. Otherwise, a Keyence VK-X1000 confocal microscope system was used to inspect the Fe-SMA strips after fracture. Thus, the bare metal was distinguishable from the thin adhesive layers. A Keyence VR-5000 wide-area 3D measurement system was used for the large-area scans, as in Fig. 5a. The amount of cohesive failure was measured using the image analysis tool ImageJ [41]. The ratio of white to total pixels was measured using the color threshold and de-noise feature to separate the bare metal from the rest (Fig. 5b).

Using ImageJ and the VR-5000 images, the depth of the edge debonding owing to water infiltration for the aged samples was also measured (Fig. 5a). The debonding depth is clearly recognizable as the transition from full adhesive failure to either cohesive or mixed failure modes. With the Sika adhesive, it was possible to visually measure the edge debonding depth, even in the case of complete adhesive failure. The two regions were clearly visible on the Fe-SMA fracture surfaces as a color change in Fig. 6. The edge-debonded area was not considered in the computation of the percentage of cohesive failure, as this would introduce a size effect.

2.5.3. FTIR

Using microscope analysis, visual detection of bare metal was possible, but an interfacial failure between the primer and adhesive could be misclassified as a cohesive failure. In both cases, the underlying metal would not be visible. This issue was addressed by FTIR spectroscopy using a PerkinElmer Spectrum 100 spectrometer.

With Hysol prepared with sol–gel and either primer, the fracture surfaces exhibited regions where the Hysol adhesive was recognizable through microscopy and regions where a thin light yellow layer covered the metal (Fig. 7b). To determine whether this was an exposed primer, pure adhesive and pure primer FTIR spectra were measured. Both materials were analyzed three times to produce the spectra presented in Fig. 7a. Between 3100 and 2700 cm^{-1}, a clear difference in spectral shape is recognizable, which is generally attributed to epoxy groups.

Finally, the experimental fracture surface showing an undetermined failure mode was measured at 20 different locations in the focus range. The relative crystal size is shown in Fig. 7b. None of the recorded spectra presented the characteristic shape of the primer spectrum, and the Hysol peak at 2821 cm^{-1} is present in all measurements. The thin yellow layer could be identified as Hysol adhesive, and it was thus concluded that the failure occurred cohesively in these regions as well. This was the case for all surface preparations involving Hysol, sol–gel and either primer.

3. Results

3.1. Effect of surface preparation

The average peel load recorded for every surface preparation and adhesive is presented in Fig. 8. The secondary axis indicates the percentage of cohesive failure. The names of the surface preparations describe the succession of the applied processes (grit blasting (GB), sol–gel (SG), chromatic primer (P_C), non-chromatic primer, (P_{NC}), and UV/ozone exposure (UV)). If the test followed Scenario B or C, the bar was hatched (insert Fig. 8(a)).

The results obtained with the Sika adhesive are displayed in Fig. 8(a). The results show that surface preparation is necessary because grit blasting alone yields complete interfacial debonding. Using either primer or UV/ozone exposure was not sufficient to obtain cohesive failure either. However, it appears that the addition of sol–gel to the primer yields a 100% cohesive failure along with a significant increase in peel load. All tests followed Scenario A, even with adhesive failure. Very high loads were reached with this adhesive compared to the other adhesives.

In the case of Araldite (Fig. 8(b)), the most striking result is that grit blasting alone produces complete cohesive failure. It appears that the

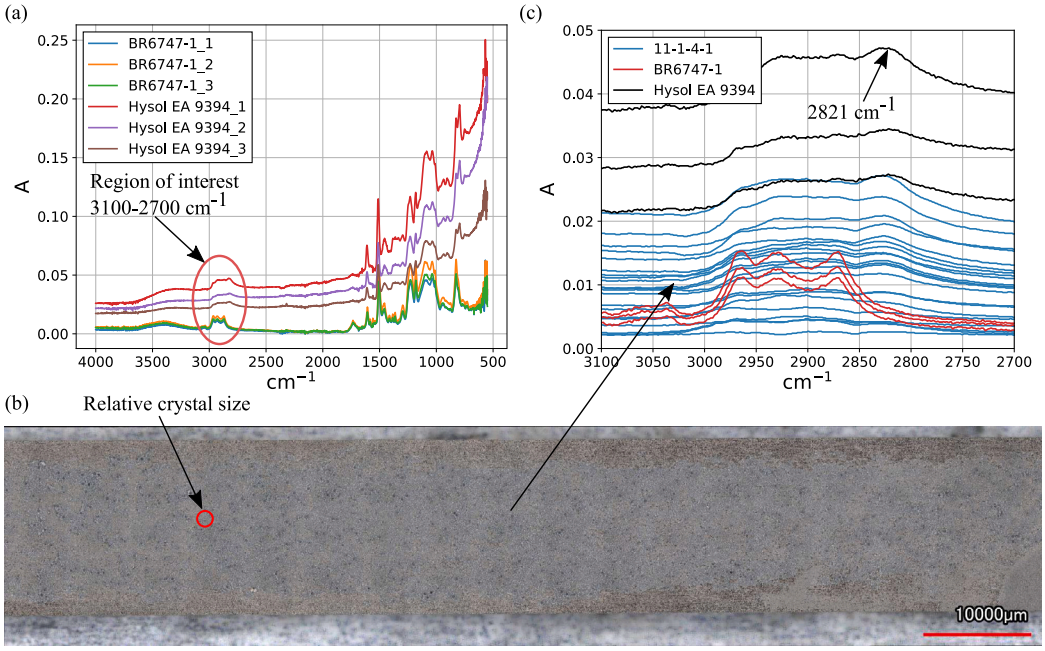

Fig. 7. (a) FTIR spectrum for pure Hysol adhesive and pure primer P_C. (b) Fe-SMA fracture surface bonded with Hysol prepared with GB+SG+P_C. Areas showing a thick layer of adhesive are recognizable by the characteristic gray color. Areas with thinner layers are yellow. (c) FTIR spectra in the focus range at 20 random locations on the fracture surface, along with both adhesive and primer spectra.

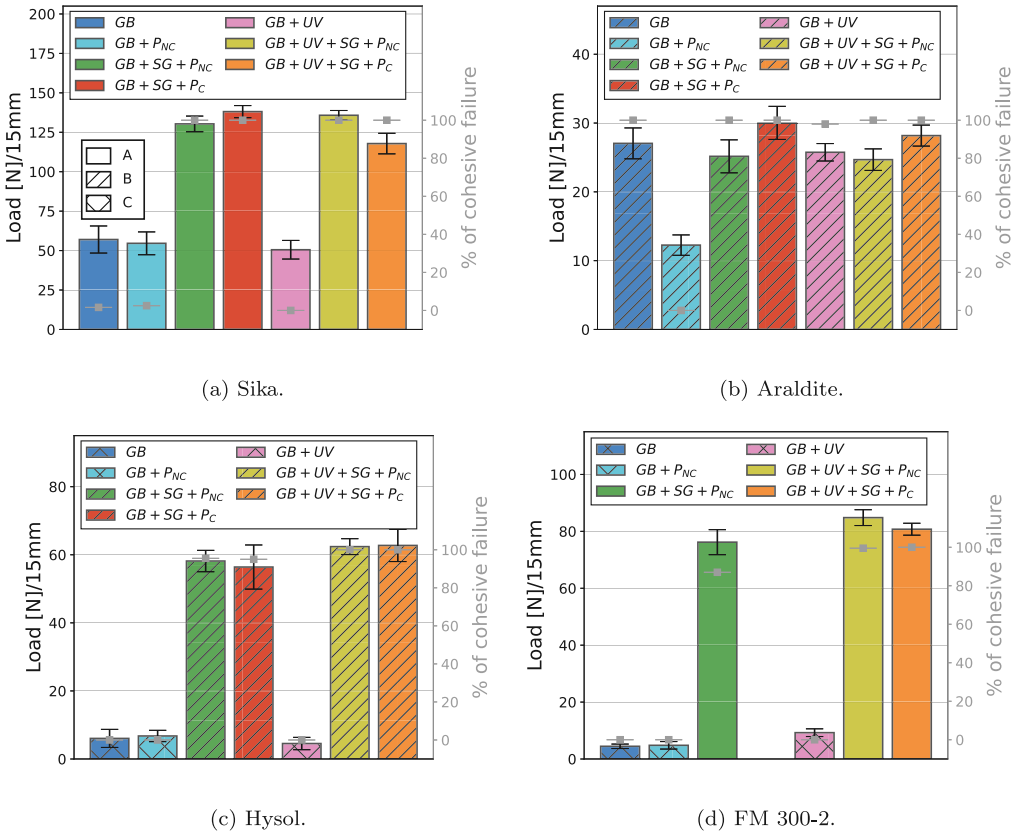

(a) Sika.

(b) Araldite.

(c) Hysol.

(d) FM 300-2.

Fig. 8. Peel load and percentage of cohesive failure for every adhesive as function of the surface preparation. The percentage of cohesive failure over the total crack surface is in gray. A, B, and C in (a) refer to Fig. 3. GB stands for grit blasting, SG is the sol–gel, P_{NC} is the non-chromatic primer, P_C is the chromatic primer, and UV is the UV/ozone treatment.

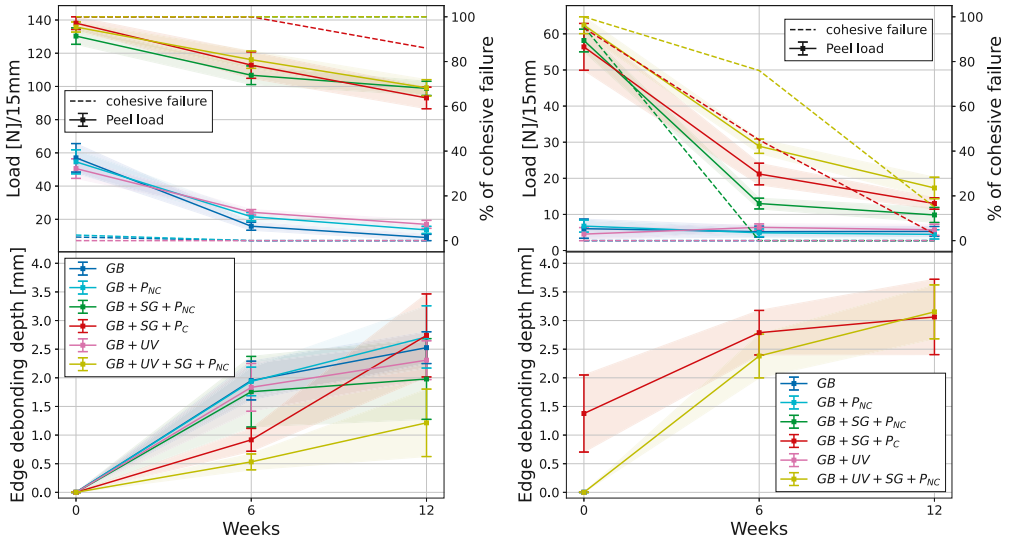

(a) Effect of aging Sika. (b) Effect of aging Hysol.

Fig. 9. Effect of aging in the salt spray cabinet on the joints.

non-chromatic primer alone has a negative effect on adhesion, leading to complete adhesive failure and accordingly lower peel load. These results were repeated to eliminate the possibility of contamination during manufacturing, and the results were consistent. In addition, the test followed Scenario B (Fig. 3(b)).

The Hysol results are presented in Fig. 8(c). In the case of GB, GB+P_{NC}, and GB+UV, the test followed Scenario C. The Fe-SMA did not comply with the roller and resulted in a limited deformation of the Fe-SMA after the test, along with 0 % cohesive failure. In these cases, the reported peel load cannot be compared with the others. For the three surface preparations involving sol–gel, the peel tests followed Scenario B (Fig. 3(b)) and failed mostly cohesively.

Finally, the FM 300-2 results, presented in Fig. 8(d) are similar to the Hysol results. Only showing that the extra cleaning and oxidation step provided by the UV/ozone improved cohesive failure percentage when used with sol–gel and the non-chromatic primer. It was not possible to test GB+SG+P_C as evidence of surface contamination was observed on the samples, and the results were not reported.

3.2. Effect of aging

Aging had a negative effect on the integrity of bonded joints. The peel load decreased consistently, as displayed in the top part of the plots with the filled lines in Fig. 9. As a second effect, the percentage of cohesive failure decreased (dashed lines on the top plots in Fig. 9). Third, the joints exhibited edge debonding (Fig. 5a and Fig. 6).

Fig. 9(a) shows the effect of the salt spray exposure on the Sika joints. The two groups visible in Fig. 8(a) are also visible here. The preparations yielding cohesive failure (all with sol–gel) retained most of this characteristic (only the chromatic primer preparation showed some loss of cohesive failure), while the peel loads dropped linearly to 72 ± 3.5 % of their initial value after 12 weeks. Furthermore, for the surface preparation yielding adhesive failure before aging, the load decreased significantly to reach $16, 24, 33\%$ (in order of appearance) of their initial values after 12 weeks. The least performing surface preparations, those without sol–gel, also performed less in durability.

In the lower plot of Fig. 9(a), the debonding depth as a function of the exposure time is represented. All joints exhibited comparable debonding depths after 12 weeks, with the exception of GB+UV+SG+P_{NC}, showing 60% less debonding after 12 weeks.

In the case of Hysol, aging in the salt spray cabinet had a significant effect on the joint, as shown in Fig. 9(b). Indeed, the preparations showing cohesive failure before aging (those with sol–gel) showed a decrease in peel load to below 30% of their initial value. Meanwhile, the cohesive failure was lost completely, except for GB+UV+SG+P_{NC}, which retained 15% of cohesive failure. As for the edge effect, only the two preparations showing cohesive failure were measured and reported. The two curves reported in Fig. 9(b) show similar results. The debonding after 0 weeks was due to damage caused by waterjet cutting.

4. Discussion

In this study, a large array of surface preparation methods and four adhesives were tested when bonded to Fe-SMA. It is shown that for the four selected adhesives, complete cohesive failure can be guaranteed prior to aging. In the second step, the durability of certain joints was tested by accelerated salt-spray aging. Sika and Hysol adhesives were investigated, and several mechanisms of joint degradation were identified. In this section, several aspects of the results are discussed to provide additional insight into the analysis.

4.1. Influence of surface preparations

From Fig. 8, it appears that sol–gel AC-130 is the crucial preparation step that allows to reach complete cohesive failure for Sika, Hysol, and FM 300-2. Without this, none of these adhesives bonded properly to the Fe-SMA surface.

To isolate the effect of the sol–gel from the primer, the surface was prepared with primer alone. For all adhesives, only applying the primer had no effect compared to grit blasting only, and even a negative effect on the Araldite adhesion (blue and cyan bar in Fig. 8(b)). It appears that the primer does not adhere to the Fe-SMA on its own, making the sol–gel step the most important in ensuring adhesion between the primers and the surface.

Furthermore, in Fig. 9(a), it appears that the primer alone does not improve the bond's durability either. The peel load and water penetration depth were similar to the bonds with grit blasting only. This further emphasizes the importance of the sol–gel in terms of durability and evidences the incompatibility between the primer and the Fe-SMA.

The next interlayer in Fig. 1c is the primer. Two versions of the same primer were used in this study, the non-chromatic one being an environmentally friendlier alternative version of the regular BR6747-1. From Fig. 8, no difference can be noted between the two primers

prior to aging. As chromium is a key element in corrosion protection, its absence can affect primer performance in aging. Nonetheless, in the case of the Sika joints (see Fig. 9(a)), both the red (chromatic primer) and green (non-chromatic) curves show similar behavior with respect to the loss of peel load.

In the lower plot of Fig. 9(a), both primers showed similar debonding of the edges as surface preparations without primer. It seems that the primer does not protect the exposed edges from water ingress. It preserved cohesive failure in the middle of the joint and protected the interface from water in the adhesive, but did not affect edge debonding.

With Hysol, Fig. 9(b), the non-chromatic primer did not prevent a complete loss of cohesive failure after six weeks, whereas the chromatic version allowed 45 % cohesive failure. Accordingly, the peel load using the chromatic primer was higher than that of the non-chromatic version. However, both show only 22 % and 37 % of their respective initial peel loads after six weeks, which cannot be considered acceptable.

The third surface preparation step investigated was the UV/ozone exposure, which was used on grit blasted Fe-SMA and in combination with sol–gel and primer (Fig. 8). Its effect on durability was tested only in combination with the non-chromatic primer. With regard to the use of UV/ozone alone, no significant effect was observed compared to grit blasting alone.

When used in combination with sol–gel and primer, UV/ozone exposure allowed to reach complete cohesive failure if not already obtained with sol–gel and primer. This was the case for Hysol (Fig. 8(c)) and FM 300-2 (Fig. 8(d)), where the peel load increased accordingly. This is likely induced by better wetting of the surface by the sol–gel allowed by the exposure (Fig. 2(b)).

The UV/ozone exposure showed a significant improvement in durability. The surface preparation GB+UV+SG+P_{NC} showed the least joint deterioration (Fig. 9). The edge debonding is 70% and 40% less deep after 6 and 12 weeks than the same preparation without UV. With Hysol, it was the only surface preparation that retained some amount of cohesive failure. Again, it is assumed that the improved wetting of the Fe-SMA by the sol–gel prevented water from propagating at the interface.

4.2. Adhesive comparison

Four adhesives were investigated and all were compatible with both primers, as no evidence of interfacial failure between the primers and the adhesives was observed (see Fig. 7,Section 2.5.3).

In complete adhesive failure, Sika and Araldite followed Scenarios A and B. The peel loads were 57 N/15 mm, and 12 N/15 mm, namely 41 % and 40 % of their cohesive failure peel load, respectively. In complete adhesive failure, the two other adhesives showed no adhesion at all as they followed Scenario C. Both Sika and Araldite are ductile adhesives (Table 1) and a partial plastification of the adhesive diffused energy, resulted in a higher load. Brittle adhesives can only diffuse energy through fracture, which does not occur.

Regarding durability, it is evident that the Hysol joint suffered severe degradation (Fig. 9(b)). Aakkula et al. [18] tested lap-shear AISI 304 grade steel joints bonded with Hysol EA 9396 (the unfilled version of EA 9394 used in this study) prepared with the same chromatic primer and sol–gel. It was found that cohesive failure occurred after 30 days of exposure to a hot wet environment (60 ° C/98 % RH). While the materials used for surface preparation were the same, the adherend material, the grit blasting parameters, and mechanical test were different. While peel tests are considered more severe for the interface than shear loading, it is assumed that the incompatibility between the Fe-SMA and the primer might be the source of this poor durability.

The joints using Sika adhesive (Fig. 9(a)) in combination with an appropriate surface preparation showed signs of degradation, namely debonding at the edges, but no loss of cohesive failure in the middle of the joint. This highlights the importance of protecting the joint from water infiltration, but indicates that the joint is durable and sustains its strength when exposed to harsh conditions.

4.3. Test scenarios

As mentioned in Section 2.4.1, the peel test does not systematically follow Scenario A; therefore, the peel load results are not comparable. For a crosshead displacement $\Delta_{machine}$ with load P per unit depth, the debonding will advance ΔA, and the extra energy $P\Delta_{machine}$ is distributed according to the following expression:

$$P\Delta_{machine} = G\Delta A + \Delta W_e + \Delta U_{diss} \tag{1}$$

where G is the joint critical energy release rate (ERR) assumed homogeneous in the specimen length direction, ΔW_e is the elastic energy stored in the newly debonded flexible strip, and ΔU_{diss} is the energy dissipated (via plasticity and phase transformation in the Fe-SMA) in the same volume. Assuming that the test has reached a steady-state, meaning each newly debonded strip undergoes the same deformation history as previously debonded strip, a constant peel load, P, is necessary to propagate the crack as shown in Fig. 4:

$$P = G\underbrace{\frac{\Delta A}{\Delta_{machine}}}_{\text{constant}\sim 1} + \underbrace{\frac{\Delta W_e}{\Delta_{machine}} + \frac{\Delta U_{diss}}{\Delta_{machine}}}_{\text{constant but depending on scenario}} \tag{2}$$

It is evident that the peel loads are not a direct measure of the joint strength, and the comparison is invalid between different scenarios. To address this issue, an alternative fixture design constraining the specimen to Scenario A along with a complete energetic analysis of the alternative fixture was proposed by Kemp [38].

Using the floating-roller fixture and a simplified strip material behavior, Kawashita [42] also proposed a complete energy analysis of the test when following Scenario A, and reported a fourth possible test scenario, that is, when the crack front moves forward owing to the high adhesion to adherend stiffness ratio. The plastic bending energy contributed up to 75 to 90 % of the peel load. Hence, the difference due to plastic deformation in Scenarios A, B, and C can be a major contributor to the decrease in load, while not allowing to conclude on variations in G.

4.4. General discussion

It appeared that the flexible 0.5 mm thickness Fe-SMA strips were slightly too stiff to comply with the fixture. As discussed in the previous section, the peel load is influenced by plastic and phase transformation deformation, which can vary from test to test. The results are therefore qualitative in nature, and no fracture toughness of the bond was measured with the peel test. Nonetheless, the objective is to investigate the compatibility of surface preparation materials, adhesives, and Fe-SMA to obtain cohesive failure. The test setup was adopted owing to its simplicity, rapid execution, allowing for an extensive test matrix such as the one in Table 3, and its asymmetry allowing to test only the Fe-SMA-adhesive interface. This was confirmed experimentally as none of the test exhibited interfacial failure between the AISI 304 grade steel and adhesive.

While the methods investigated in the current study are so far confined to aerospace applications, the findings of this paper are meaningful for civil engineering (the current field of application of the Fe-SMA) applications as well. The proposed surface preparation is relatively easy and involves no work on the application site as the primer has a surface stabilization function that allows prepared surfaces to be stored up to 6 month prior to bonding [33].

Lastly, it is worth mentioning an important influencing parameter left out of this study. Namely the effect of prestraining of the Fe-SMA. This limitation has multiple implications as the prestraining can affect the local interface as well as the global mechanical behavior. Martensitic transformation induces an out of plane deformation at the free surface and will affect the free surface roughness [34]. Even if this was not investigated specifically for the ε martensite forming in the

Fe-SMA, it is fair to assume this effect also occurs in the alloy. This can have a major effect on the bond properties as martensite is formed during the sandblasting and the prestraining steps. This is however outside of the scope of this paper focusing only on the 2% prestrain level and left for future studies.

The prestraining level can have significant influence on the joint durability. Indeed, the corrosion resistance of the Fe-SMA is influenced by the deformation [43]. Up to 4 % prestrain, no significant influence was observed but a pronounced decrease was observed beyond this threshold [44].

Finally, the prestraining level and martensitic volume fraction has an influence on the Fe-SMA mechanical properties, which influences the peel load. The current test is not appropriate as the Fe-SMA mechanical behavior is influenced by the prestrain and therefore an alternative test procedure such as the butt-tension test (ASTM D2095-96 [45]) shall be used to investigate this parameter.

5. Conclusion

The effect of surface preparation methods including UV/ozone exposure, sol–gel, and primer on the adhesion and durability of an adhesively-bonded Fe-SMA was investigated. Bonded joints were subjected to a peel load applied through the floating-roller peel test, and the load and failure modes were reported. The main findings of this study are as follows:

1. For all selected adhesives, complete cohesive failure of bonded Fe-SMA joints was obtained. Sol–gel and primers are needed to improve the Fe-SMA-adhesive interface strength for SikaPower 1277, Hysol EA 9394, and FM 300-2 adhesive film. No surface preparation was required for Araldite 2015.
2. The application of sol–gel AC 130-2 is the crucial step to achieve cohesive failure as it was found indispensable for the primer bond with the Fe-SMA.
3. UV/ozone cleaning/surface activation helped to obtain complete cohesive failure when sol–gel and primer alone were not sufficient with FM 300-2.
4. Both primers tested showed similar performance in adhesion enhancement suggesting that the non-chromatic equivalent is a suitable alternative while being less toxic. None of the four tested adhesives were incompatible with the primers.
5. Even in adhesive failure, ductile adhesives SikaPower 1277 and Araldite 2015 resisted peel while the brittle adhesives FM 300-2 and Hysol EA 9394 did not.
6. The accelerated aging of the joints revealed the effect of the corrosion protection of the adherends.
    (a) SikaPower 1277 combined with sol–gel and either primer exhibited limited deterioration. The UV/ozone exposure reduced the edge debonding depth by 30 % after 12 weeks.
    (b) Hysol EA 9394 joints using sol–gel and either primers lost all of the cohesive failure after 12 weeks and the load decreased accordingly.

Declaration of competing interest

The authors declare that they have no known competing financial interests or personal relationships that could have appeared to influence the work reported in this paper.

Data availability

No data was used for the research described in the article

Acknowledgments

The authors would like to acknowledge the financial support of the Swiss National Foundation, SNSF, Switzerland (Grant No. 200021_192238), as well as Huntsmann Advanced Materials (Switzerland) GmbH, re-fer AG and Sika for providing material used for this work. Special thanks to Dr. Sofia Teixeira de Freitas, the staff of the Delft Aerospace Structures and Materials Laboratory and the DEMO University workshop for their kind support.

References

[1] Ghafoori E, Hosseini E, Leinenbach C, Michels J, Motavalli M. Fatigue behavior of a Fe-Mn-Si shape memory alloy used for prestressed strengthening. Mater Des 2017;133:349–62. http://dx.doi.org/10.1016/j.matdes.2017.07.055.
[2] Izadi M, Hosseini A, Michels J, Motavalli M, Ghafoori E. Thermally activated iron-based shape memory alloy for strengthening metallic girders. Thin-Walled Struct 2019;141:389–401. http://dx.doi.org/10.1016/j.tws.2019.04.036.
[3] Fritsch E, Izadi M, Ghafoori E. Development of nail-anchor strengthening system with iron-based shape memory alloy (Fe-SMA) strips. Constr Build Mater 2019;229:117042. http://dx.doi.org/10.1016/j.conbuildmat.2019.117042.
[4] Wang W, Li L, Hosseini A, Ghafoori E. Novel fatigue strengthening solution for metallic structures using adhesively bonded Fe-SMA strips: A proof of concept study. Int J Fatigue 2021;148:106237. http://dx.doi.org/10.1016/j.ijfatigue.2021.106237.
[5] Shahverdi M, Michels J, Czaderski C, Motavalli M. Iron-based shape memory alloy strips for strengthening RC members: Material behavior and characterization. Constr Build Mater 2018;173:586–99. http://dx.doi.org/10.1016/j.conbuildmat.2018.04.057.
[6] Hosseini E, Ghafoori E, Leinenbach C, Motavalli M, Holdsworth SR. Stress recovery and cyclic behaviour of an Fe–Mn–Si shape memory alloy after multiple thermal activation. Smart Mater Struct 2018;27(2):025009. http://dx.doi.org/10.1088/1361-665X/aaa2c9.
[7] Izadi M, Ghafoori E, Shahverdi M, Motavalli M, Maalek S. Development of an iron-based shape memory alloy (Fe-SMA) strengthening system for steel plates. Eng Struct 2018;174:433–46. http://dx.doi.org/10.1016/j.engstruct.2018.07.073.
[8] Izadi M, Ghafoori E, Motavalli M, Maalek S. Iron-based shape memory alloy for the fatigue strengthening of cracked steel plates: Effects of re-activations and loading frequencies. Eng Struct 2018;176:953–67. http://dx.doi.org/10.1016/j.engstruct.2018.09.021.
[9] Wang W, Hosseini A, Ghafoori E. Experimental study on Fe-SMA-to-steel adhesively bonded interfaces using DIC. Eng Fract Mech 2021;244:107553. http://dx.doi.org/10.1016/j.engfracmech.2021.107553.
[10] Petrie EM. Handbook of adhesives and sealants. New York; London: McGraw-Hill; 2007, OCLC, 1159417984.
[11] Kwakernaak A, Hofstede J, Poulis J, Benedictus R. Improvements in bonding metals (steel, aluminium). In: Advances in structural adhesive bonding. Elsevier; 2010, p. 185–236. http://dx.doi.org/10.1533/9781845698058.2.185.
[12] Teng JG, Fernando D, Yu T, Zhao XL. Treatment of steel surfaces for effective adhesive bonding. In: Ye L, Feng P, Yue Q, editors. Advances in FRP composites in civil engineering. Berlin, Heidelberg: Springer Berlin Heidelberg; 2011, p. 865–8. http://dx.doi.org/10.1007/978-3-642-17487-2_190.
[13] Fernando ND. Bond behaviour and debonding failures in CFRP-strengthened steel members, 369.
[14] Man H, Zhao N. Enhancing the adhesive bonding strength of NiTi shape memory alloys by laser gas nitriding and selective etching. Appl Surf Sci 2006;253(3):1595–600. http://dx.doi.org/10.1016/j.apsusc.2006.02.057.
[15] Bouquet F, Cuntz J, Coddet C. Influence of surface treatment on the durability of stainless steel sheets bonded with epoxy. J Adhes Sci Technol 1992;6(2):233–42. http://dx.doi.org/10.1163/156856192X00304,.
[16] Blohowiak KY, Osborne H. Sol-gel coated metal, US005939197A, 21, URL https://patents.google.com/patent/US5939197A/en.
[17] Meyer S, Schubert U, De Bardi M, Wiesinger R, Schreiner M, Grohmann T. Adhesion pretreatment of aluminum by sol–gel processing. Int J Adhes Adhes 2014;51:103–10. http://dx.doi.org/10.1016/j.ijadhadh.2014.02.015.
[18] Aakkula J, Saarela O. Silane based field level surface treatment methods for aluminium, titanium and steel bonding. Int J Adhes Adhes 2014;48:268–79. http://dx.doi.org/10.1016/j.ijadhadh.2013.09.039.
[19] Ghafoori E, Neuenschwander M, Shahverdi M, Czaderski C, Fontana M. Elevated temperature behavior of an iron-based shape memory alloy used for prestressed strengthening of civil structures. Constr Build Mater 2019;211:437–52. http://dx.doi.org/10.1016/j.conbuildmat.2019.03.098.
[20] D14 Committee. Test method for floating roller peel resistance of adhesives. Tech. rep., ASTM International, http://dx.doi.org/10.1520/D3167-10R17.
[21] de Freitas ST, Sinke J. Adhesion Properties of Bonded Composite-to-Aluminium Joints Using Peel Tests. J Adhes 2014;90(5–6):511–25. http://dx.doi.org/10.1080/00218464.2013.850424,.

[22] Arouche MM, Budhe S, Alves LA, Teixeira de Freitas S, Banea MD, de Barros S. Effect of moisture on the adhesion of CFRP-to-steel bonded joints using peel tests. J Braz Soc Mech Sci Eng 2018;40(1):10. http://dx.doi.org/10.1007/s40430-017-0959-6,.
[23] Arouche MM, Budhe S, Banea MD, Teixeira de Freitas S, de Barros S. Interlaminar adhesion assessment of carbon-epoxy laminates under salt water ageing using peel tests. Proc Inst Mech Eng L 2019;233(8):1555–63. http://dx.doi.org/10.1177/1464420718766626,.
[24] G01 Committee. Practice for operating salt spray (fog) apparatus. ASTM International, http://dx.doi.org/10.1520/B0117-19.
[25] Mohri M, Ferretto I, Leinenbach C, Kim D, Lignos DG, Ghafoori E. Effect of thermomechanical treatment and microstructure on pseudo-elastic behavior of Fe–Mn–Si–Cr–Ni-(V, C) shape memory alloy. Mater Sci Eng A 2022;855:143917. http://dx.doi.org/10.1016/j.msea.2022.143917.
[26] Dong Z, Klotz UE, Leinenbach C, Bergamini A, Czaderski C, Motavalli M. A Novel Fe-Mn-Si Shape Memory Alloy With Improved Shape Recovery Properties by VC Precipitation. Adv Energy Mater 2009;11(1–2):40–4. http://dx.doi.org/10.1002/adem.200800312,.
[27] Henkel Corporation, Hysol® EA 9394, Epoxy Paste Adhesive. 2002.
[28] Sika, SikaPower®-1277, Product data sheet. 2019.
[29] Ceytec engineered materials, FM® 300-2 Film Adhesive, Technical data sheet. 2011.
[30] Huntsman, Araldite® 2015-1 structural adhesives, Technical datasheet. 2017.
[31] 3M Surface Pre-Treatment AC-130, Technical data sheet. 2012.
[32] Solvay, Technical DATA SHEET, BR 6747-1NC PRIMER. 2017.
[33] Ceytec engineering materials BR 6747-1 bonding primer, Technical data sheet. 2010.
[34] Porter DA. Phase transformations in metals and alloys. 3rd ed. Boca Raton, FL: CRC Press; 2009, OCLC, 908093351,
[35] Vig JR. UV/ozone cleaning of surfaces. J Vac Sci Technol A 1985;3(3):1027–34. http://dx.doi.org/10.1116/1.573115,.
[36] Ardila-Rodríguez LA, Boshuizen B, Rans C, Poulis JA. The influence of grit blasting and UV/Ozone treatments on Ti-Ti adhesive bonds and their durability after sol-gel and primer application. Int J Adhes Adhes 2021;104:102750. http://dx.doi.org/10.1016/j.ijadhadh.2020.102750.
[37] DePalo NA, Kodali SP, Curley RC. The Effect of Primer Thickness and Cure on the Bond Strength of a Nitrile-Phenolic Adhesive System. 1981, 811101. http://dx.doi.org/10.4271/811101.
[38] Kemp RD. A study of the floating roller peel test for adhesives, 68.
[39] Ardila-Rodríguez LA, Rans C, Poulis JA. Effect of surface morphology on the Ti–Ti adhesive bond performance of Ti6Al4V parts fabricated by selective laser melting. Int J Adhes Adhes 2021;110:102918. http://dx.doi.org/10.1016/j.ijadhadh.2021.102918.
[40] Lopes Fernandes R, Teixeira de Freitas S, Budzik MK, Poulis JA, Benedictus R. Role of adherend material on the fracture of bi-material composite bonded joints. Compos Struct 2020;252:112643. http://dx.doi.org/10.1016/j.compstruct.2020.112643.
[41] Schneider CA, Rasband WS, Eliceiri KW. NIH Image to ImageJ: 25 years of image analysis. Nature Methods 2012;9(7):671–5. http://dx.doi.org/10.1038/nmeth.2089,.
[42] Kawashita LF, Moore DR, Williams JG. Comparison of Peel Tests for Metal–Polymer Laminates for Aerospace Applications. J Adhes 2005;81(6):561–86. http://dx.doi.org/10.1080/00218460590954557,.
[43] Söderberg O, Liu X, Yakovenko P, Ullakko K, Lindroos V. Corrosion behaviour of Fe–Mn–Si based shape memory steels trained by cold rolling. Mater Sci Eng A 1999;273–275:543–8. http://dx.doi.org/10.1016/S0921-5093(99)00396-2.
[44] Lee WJ, Partovi-Nia R, Suter T, Leinenbach C. Electrochemical characterization and corrosion behavior of an Fe-Mn-Si shape memory alloy in simulated concrete pore solutions: Corrosion of Fe-Mn-Si shape memory alloy for civil engineering. Mater Corros 2016;67(8):839–46. http://dx.doi.org/10.1002/maco.201508701.
[45] D14 Committee. Test method for tensile strength of adhesives by means of bar and rod specimens. Tech. rep., ASTM International, http://dx.doi.org/10.1520/D2095-96R15.